Comparison of Landsat-7 Enhanced Thematic Mapper Plus (ETM+) and Earth Observing One (EO-1) Advanced Land Imager

Jeffrey A. Pedelty, MEMBER SPIE
NASA Goddard Space Flight Center
Code 923
Greenbelt, Maryland 20771

Jeffrey T. Morisette
James A. Smith, FELLOW SPIE
NASA Goddard Space Flight Center
Code 920
Greenbelt, Maryland 20771

Abstract. We compare images from the Enhanced Thematic Mapper Plus (ETM+) sensor on Landsat-7 and the Advanced Land Imager (ALI) instrument on Earth Observing One (EO-1) over a test site in Rochester, New York. The site contains a variety of features, ranging from water of varying depths, deciduous/coniferous forest, grass fields, to urban areas. Nearly coincident cloud-free images were collected one minute apart on 25 August 2001. We also compare images of a forest site near Howland, Maine, that were collected on 7 September 2001. We atmospherically corrected each pair of images with the Second Simulation of the Satellite Signal in the Solar Spectrum (6S) atmosphere model, using aerosol optical thickness and water vapor column density measured by *in situ* Cimel sun photometers within the Aerosol Robotic Network (AERONET), along with ozone density derived from the Total Ozone Mapping Spectrometer (TOMS) on the Earth Probe satellite. We present true-color composites from each instrument that show excellent qualitative agreement between the multispectral sensors, along with gray-scale images that demonstrate a significantly improved ALI panchromatic band. We quantitatively compare ALI and ETM+ reflectance spectra of a grassy field in Rochester and find $\leqslant 6\%$ differences in the visible/near infrared and $\sim 2\%$ differences in the short-wave infrared. Spectral comparisons of forest sites in Rochester and Howland yield similar percentage agreement except for band 1, which has very low reflectance. Principal component analyses and comparison of normalized difference vegetation index histograms for each sensor indicate that the ALI is able to reproduce the information content in the ETM+ but with superior signal-to-noise performance due to its increased 12-bit quantization. © *2004 Society of Photo-Optical Instrumentation Engineers.*
[DOI: 10.1117/1.1651556]

1 Introduction

The Earth Observing One (EO-1) satellite was launched from Vandenberg Air Force Base on 21 November 2000 as the first Earth observing platform of NASA's New Millennium Program. As part of this effort, NASA formed a Science Validation Team (NRA 99-OES-01, EO-1) to contrast and compare the new sensor technologies with proven sensors such as the Enhanced Thematic Mapper Plus (ETM+) on the Landsat-7 spacecraft.[1] In this paper we present some of our comparisons of the Advanced Land Imager (ALI) and the ETM+ as part of this effort. Additionally, EO-1 carried Hyperion, an advanced hyperspectral sensor.[1]

The Advanced Land Imager on the EO-1 spacecraft is a technology verification instrument under NASA's New Millennium Program. It is designed to demonstrate comparable or improved Landsat spatial and spectral resolution with substantial mass, volume, and cost savings. The EO-1 spacecraft is in the same 705-km altitude orbit as Landsat-7, and is approximately one minute behind. The ALI is a pushbroom sensor with wide-angle optics that provide for 30-m multispectral and 10-m panchromatic ground sample distance (GSD) across the same 185-km swath width as the ETM+. However, only a portion of the focal plane was populated with detectors. Each of four sensor chip assemblies views 9.6 km, resulting in an effective total swath width of 37 km after accounting for overlap. Massachusetts Institute of Technology Lincoln Laboratory developed the ALI, Santa Barbara Remote Sensing (SBRS) provided the focal plane system, and Sensor Systems Group, Inc. provided the optics.

The ETM+ on Landsat-7 is a derivative of the Thematic Mapper sensors that were flown on Landsats 4 and 5 beginning in 1982. It is more closely related to the Enhanced

Thematic Mapper (ETM) that was lost in the launch failure of the commercial Landsat-6 in 1993. The primary changes from the TM sensors are the addition of a 15-m panchromatic band, the incorporation of two gain ranges for all bands, the improvement of the thermal band spatial resolution to 60 m, and the addition of two solar calibrators.[2,3] The ETM+ was built by SBRS under contract to NASA.

The ALI differs from the ETM+ in a number of ways. The pushbroom design of the ALI provides a much longer dwell time per pixel (~4 msec) than the whiskbroom ETM+ (~10 μsec), which permits 12-bit digitization of the ALI data with a single gain setting. The 10-m GSD of the panchromatic band improves on the 15-m GSD of the ETM+, and the ALI panchromatic band was narrowed to 0.48–0.70 μm from the 0.52–0.90 μm bandwidth on the ETM+. The ALI also has two new multispectral bands: band 1′ (0.43–0.45 μm) and 5′ (1.20–1.29 μm). Additionally, the ETM+ band 4 was split into bands 4 and 4′ to avoid an atmospheric water absorption feature. Finally, the ALI has no thermal band.

Our paper is organized as follows. We describe the images acquired over Rochester, New York, and Howland, Maine. We used the Second Simulation of the Satellite Signal in the Solar Spectrum (6S) radiative transfer code[4] to derive coefficients for each ETM+ and ALI wavelength band that convert the at sensor radiance to estimated surface reflectance. Atmospheric parameters used by 6S were derived from nearby sun tracking photometers and from an orbiting ozone spectrometer. We extract image subsets and sample reflectance spectra to illustrate the differences and consistencies in the two sensors. Our comparisons include simple visual analyses, comparison of noise levels and spectral reflectance curves, and analysis of information content using principal components and calculation of Normalized Difference Vegetation Index (NDVI) images.

2 Production of the Comparison Scenes

2.1 ETM+ and ALI Data Acquisitions

The ETM+ and ALI instruments viewed the Rochester, New York, area nearly simultaneously on 25 August 2001. The ETM+ acquired the WRS2 path 16, row 30 scene at 15:40:12 GMT, while the ALI was approximately one

minute behind at 15:41:08 GMT. The instruments observed the Howland, Maine, area approximately 2 weeks later on 7 September 2001. The WRS2 path 11, row 28 scene was collected at 15:08:19 GMT by the ETM+ and at 15:09:15 by the ALI. We received the ALI Level 1 data product for each acquisition from the EO-1 Science Validation Facility[1] at NASA's Goddard Space Flight Center (GSFC). The ALI scenes have been radiometrically calibrated to provide scaled measurements of at sensor radiance, but they have not been geometrically corrected. We converted the ALI data to units of W/m^2/sr/μm by dividing by the scaling factor of 30. Our study areas were fully imaged by sensor chip assembly #4, and thus were affected by three inoperable detectors in band 5. We simply interpolated across these inoperable detectors.

The ETM+ data available for this study were in two different formats. For the Rochester scene we received the ETM+ L0R data product from the USGS EROS Data Center (EDC) via the EOS Data Gateway. The L0R scene is essentially a raw, but band separated, data product. We applied standard radiometric corrections to create L1R datasets using the GSFC copy of the EDC Image Assessment System. For the Howland scene we acquired the ETM+ L1G data product from EDC. The L1G product is a L1R scene that has been further geometrically calibrated to remove the effects of ETM+ scan mirror velocity variations and then reprojected to UTM coordinates using nearest neighbor resampling. Finally, each ETM+ scene was converted to measurements of at sensor radiance in units of W/m^2/sr/μm by applying the appropriate scaling for each data product. Full details of the data formats and radiometric and geometric processing are provided in the Landsat-7 Science Data Users Handbook, available at http:// landsat.gsfc.nasa.gov/

2.2 AERONET and TOMS Atmospheric Characterization

We monitored the atmospheric properties using Cimel (CIMEL Electronique, Paris, France) sun photometers that are part of the Aerosol Robotic Network (AERONET).[5] In Rochester, the sun photometer was installed on the roof of the Imaging Science building at the Rochester Institute of Technology, approximately 15 km southwest of our test site
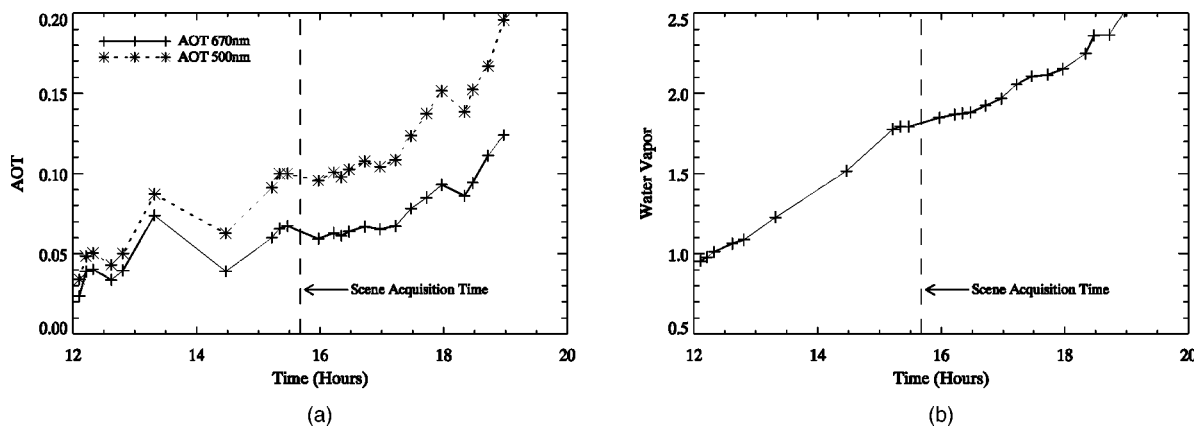

(a)

(b)

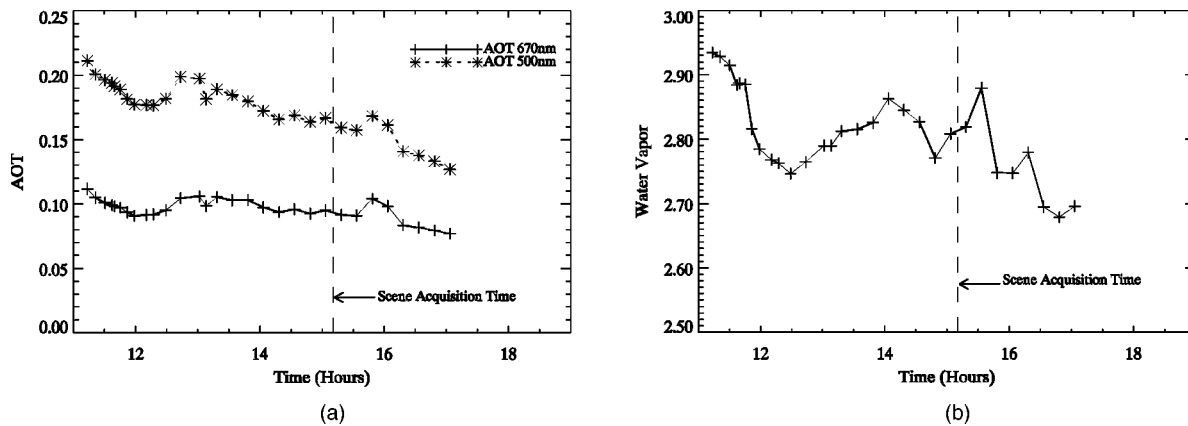**Fig. 1** AERONET retrievals for Rochester scene.

Fig. 2 AERONET retrievals for Howland scene.

at Durand Eastman Park, while the sun photometer in How-land was approximately 6 km from our test site. The sun photometers measured the aerosol optical thickness (AOT) at 670 and 500 nm and water vapor column density approximately every 15 minutes. We interpolated these AOT measurements in wavelength and time to give AOT values at 550 nm of 0.09 and 0.15 for the Rochester and Howland acquisitions, respectively. We similarly obtain a water content of 1.85 g/cm^2 and 2.81 g/cm^2 for the two scenes. In Fig. 1 (Rochester) and Fig. 2 (Howland) we show time series plots of the AERONET AOT and water vapor measurements for 8 hours spanning the acquisition times, which illustrate that the atmosphere was fairly stable at the time of our observations. We obtained total column ozone values of 0.30 cm-atm for Rochester and 0.28 cm-atm for Howland using the Earth Probe Total Ozone Mapping Spectrometer (TOMS).[6]

2.3 Atmospheric Correction Using 6S

We used these atmospheric measurements as input to the 6S radiative transfer code.[4] The 6S code calculates the atmospheric path radiance, which is the portion of the total radiance measured in each ETM+ and ALI band due to the atmosphere. The 6S code does this by calculating gaseous absorption, atmospheric scattering, and approximating the

interaction between the absorption and scattering. It integrates both the solar spectrum and the atmospheric absorption and scattering across the relative spectral response functions for each of the 17 ETM+ and ALI bands, and returns the coefficients xa, xb, and xc that convert the measured at sensor radiance in each band to atmospherically corrected surface reflectance (ACR) via the following equations:

$$y = xa * radiance - xb$$

$$ACR = y/(1 + xc * y)$$

We performed an empirical error analysis of the atmospheric correction process by also running 6S with values of AOT, water vapor, and ozone that are ±10% from their nominal values. This variation is conservative since the inversion uncertainties in the AOT values are less than 1% and the TOMS ozone values have ±3% absolute errors.[6] We will further discuss the overall uncertainty in the derived reflectances when we compare reflectance spectra in Section 3.2.

In Tables 1 and 2 we show the center wavelength, bandwidth, and the 6S-derived xa, xb, and xc correction coefficients for each of the ETM+ and ALI bands for both the

Table 1 Bandpass and atmospheric correction parameters for the VNIR bands.

	ALI 1′	ALI 1	ETM+ 1	ALI 2	ETM+ 2	ALI 3	ETM+ 3	ETM+ 4	ALI 4	ALI 4′
Center λ (μm)	0.442	0.485	0.483	0.567	0.56	0.660	0.662	0.835	0.790	0.866
Bandpass (μm)	0.43-0.45	0.45-0.51	0.45-0.52	0.53-0.60	0.53-0.61	0.63-0.69	0.63-0.69	0.78-0.90	0.78-0.80	0.84-0.89
6S results					Rochester scene					
xa	0.0032	0.0028	0.0028	0.0029	0.0029	0.0032	0.0032	0.0045	0.0039	0.0045
xb	0.1404	0.0932	0.0989	0.0507	0.0528	0.0271	0.0270	0.0119	0.0135	0.0097
xc	0.1868	0.1466	0.1520	0.0950	0.0980	0.0630	0.0627	0.0349	0.0394	0.0314
6S results					Howland scene					
xa	0.0036	0.0031	0.0031	0.0032	0.0032	0.0034	0.0035	0.0049	0.0043	0.0049
xb	0.1600	0.1070	0.1134	0.0598	0.0621	0.0331	0.0330	0.0157	0.0173	0.0127
xc	0.1954	0.1567	0.1619	0.1065	0.1095	0.0747	0.0743	0.0446	0.0497	0.0406

Table 2 Bandpass and atmospheric correction parameters for the SWIR and panchromatic bands.

	ALI 5′	ETM+ 5	ALI 5	ETM+ 7	ALI 7	ETM+ pan	ALI pan
Center λ (μm)	1.244	1.648	1.640	2.206	2.226	0.705	0.592
Bandpass (μm)	1.20-1.29	1.55-1.75	1.55-1.73	2.09-2.35	2.09-2.36	0.52-0.90	0.50-0.68
6S results				Rochester scene			
xa	0.0101	0.0199	0.0194	0.0598	0.0612	0.0036	0.0030
xb	0.0037	0.0017	0.0017	0.0007	0.0007	0.0280	0.0461
xc	0.0148	0.0080	0.0081	0.0037	0.0037	0.0618	0.0895
6S results				Howland scene			
xa	0.0110	0.0214	0.0208	0.0649	0.0664	0.0040	0.0032
xb	0.0055	0.0026	0.0026	0.0012	0.0012	0.0341	0.0544
xc	0.0210	0.0121	0.0123	0.0060	0.0059	0.0727	0.1010

Rochester and Howland scenes. In each table the first set of coefficients is for the Rochester data while the next set is for Howland.

3 Results and Discussion

3.1 *Visual Image Comparisons*

We extracted 320×320 pixel subimages from the Rochester scenes near our forest test site in the Durand Eastman Park, including Lake Ontario, Irondequoit Bay, and NE Rochester. In Fig. 3 we show true color composites (online version only) of the atmospherically corrected reflectance images using bands 3, 2, and 1 of the ETM+ and ALI. We use identical linear color transfer functions that exclude the highest and lowest 2% of the pixel histograms. We present Level 1R data from both instruments to maximize radiometric fidelity, which means that slight geometric displacements are visible in the ETM+ image due to scan mirror velocity variations, and that north is not precisely up.

Qualitatively the ETM+ and ALI images are nearly indistinguishable. We can see more detail in Lake Ontario because of the 12-bit quantization of the ALI data. Interestingly, we can use the ~1 minute separation between the images to conclude that the ship near the pier in the ETM+ image is entering Lake Ontario at roughly 24 knots.

We present comparisons of the ALI and ETM+ panchromatic bands in Figs. 4, 5, and 6. In Fig. 4 we show Irondequoit Bay and the pier into Lake Ontario and in Fig. 5 we display our Rochester forest test site. The prominent facility in the center of Fig. 5 is the VanLare Waste Water Treatment Plant, and our forest site is just below and to the left. We show a similar comparison of the Howland forest site in Fig. 6. The highway interchange shown is Interstate 95 and Maine State Highway 6. In contrast to the similarity of the multispectral comparisons, we see dramatic differences between the panchromatic bands. In Fig. 4 we see that the ALI data provide better definition of the marina and pier, and dramatically more detail in the water features of both Lake Ontario and Irondequoit Bay. In Figs. 5 and 6 we see a sharply different contrast between the forest and surrounding targets, in that the trees appear bright in the ETM+ images, but are dark in the ALI data. Three effects are responsible for the improvement in the ALI panchro-

matic images: the increase in ground sampled distance from 15 to 10 m, the increase to 12-bit quantization, and the narrowing of the spectral bandpass. The 12-bit quantization is most responsible for the improved water detail, while the

Fig. 3 True color composite comparison of Rochester scene: ETM+ (top) and ALI (bottom) (color online only).
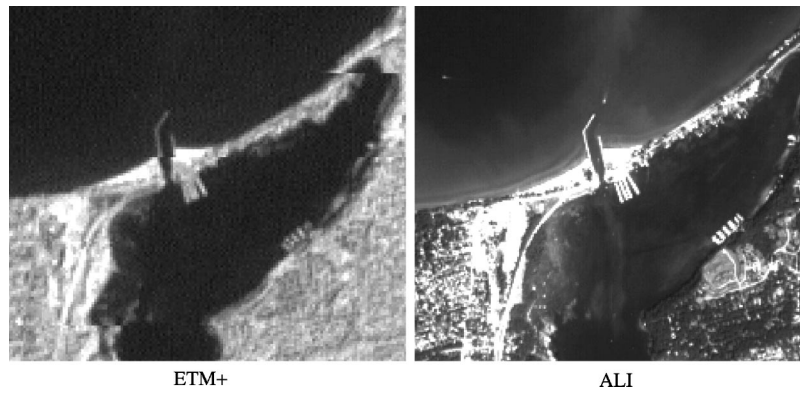
Fig. 4 Panchromatic band comparison of Irondequoit Bay and Lake Ontario.

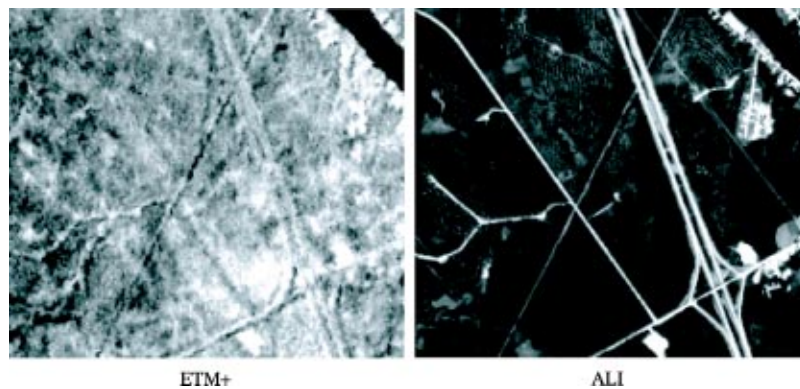**Fig. 5** Panchromatic band comparison of Durand Eastman Park site.

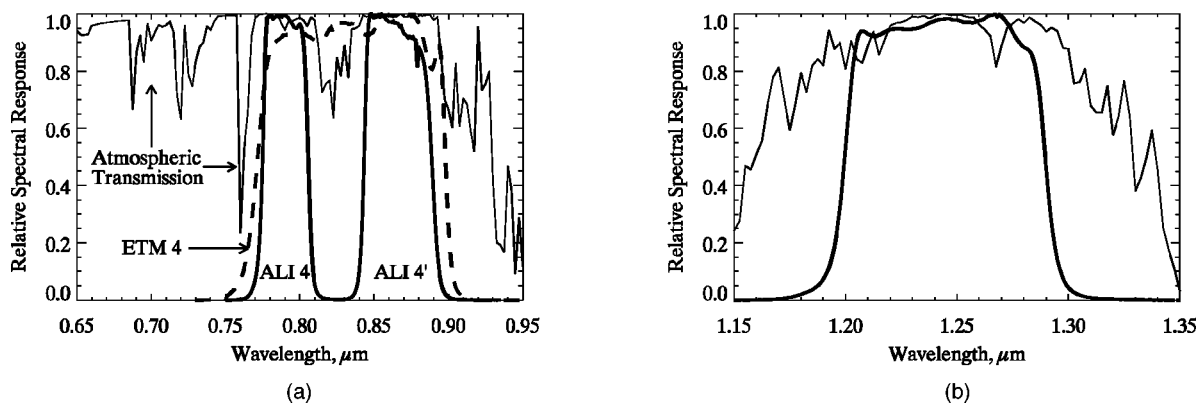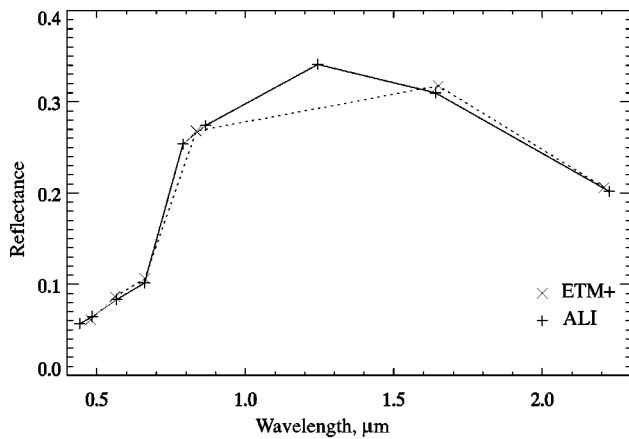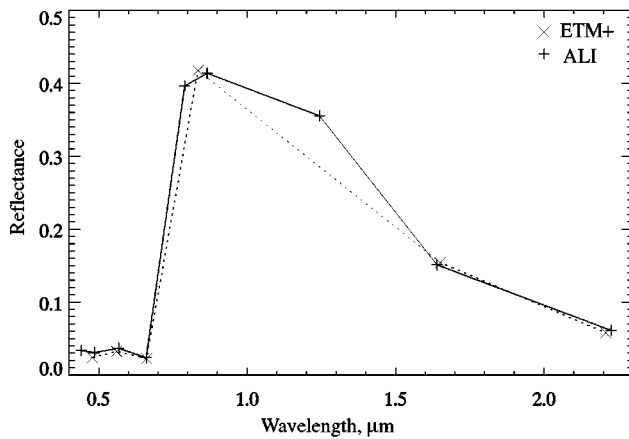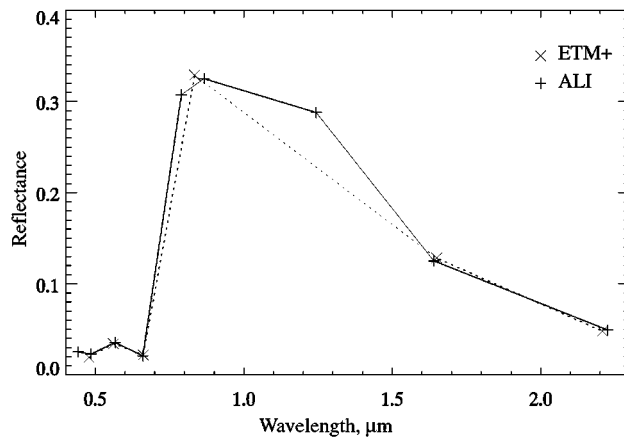**Fig. 6** Panchromatic band comparison of Howland Forest site.

Fig. 7 Comparison of ETM+ and ALI filters and atmospheric transmission.

(a)

(b)

(c)

Fig. 8 Comparison of ETM+ and ALI spectra.

narrower bandpass is more critical for the differences seen in Figs. 5 and 6. With a bandpass that cuts off at 0.7 μm, the ALI panchromatic images exclude the sharp vegetation rise, darkening the forest and improving the overall contrast.

3.2 Spectral Comparisons

The ALI was designed to acquire images in the same nominal bands as the ETM+, with the exception of the thermal

Table 3 Principal components analysis of ETM+/ALI Bands 1, 2, 3, 5, and 7 for Rochester, NY, scene.

	PCA Eigenvalues		Variation Explained	
Component #	ETM+	ALI	ETM+	ALI
1	0.0117	0.0106	91.78%	92.17%
2	0.00091	0.00081	98.94%	99.22%
3	0.000101	0.000072	99.73%	99.85%
4	0.000022	0.000010	99.91%	99.94%
5	0.000012	0.000007	100.00%	100.00%

Table 4 Principal components analysis of ETM+/ALI Bands 1, 2, 3, 5, and 7 for Howland, ME, scene.

	PCA Eigenvalues		Variation Explained	
Component #	ETM+	ALI	ETM+	ALI
1	0.00278	0.00265	90.98%	90.91%
2	0.000231	0.000238	98.53%	99.07%
3	0.000029	0.000021	99.48%	99.79%
4	0.000009	0.000004	99.77%	99.93%
5	0.000007	0.000002	100.00%	100.00%

Table 5 Principal components analysis of ETM+/ALI Bands 1, 2, 3, 4/4′, 5, and 7: eigenvalue comparison for Rochester, NY, scene.

	PCA Eigenvalues		Variation Explained	
Component #	ETM+	ALI	ETM+	ALI
1	0.0302	0.0281	87.24%	87.24%
2	0.00399	0.00380	98.77%	99.03%
3	0.00035	0.00027	99.78%	99.86%
4	0.00004	0.00003	99.90%	99.95%
5	0.00002	0.00001	99.97%	99.98%

Table 6 Principal components analysis of ETM+/ALI Bands 1, 2, 3, 4/4′, 5, and 7: eigenvalue comparison for Howland, ME, scene.

	PCA Eigenvalues		Variation Explained	
Component #	ETM+	ALI	ETM+	ALI
1	0.00636	0.00675	78.05%	79.64%
2	0.00167	0.00161	98.56%	98.64%
3	0.000114	0.000099	99.59%	99.81%
4	0.000018	0.000010	99.82%	99.93%
5	0.000009	0.000004	99.93%	99.98%

Table 7 Principal components analysis of ETM+/ALI Bands 1, 2, 3, 4/4′, 5, and 7: loadings comparison for Rochester, NY, scene.

PCA Component	PCA Loadings for ETM+ Bands						PCA Loadings for ALI Bands					
	1	2	3	4	5	7	1	2	3	4′	5	7
1	0.049	0.103	0.120	0.832	0.467	0.251	0.047	0.101	0.115	0.840	0.452	0.254
2	−0.262	−0.303	−0.403	0.495	−0.404	−0.518	−0.259	−0.309	−0.410	0.483	−0.404	−0.522
3	−0.441	−0.478	−0.441	−0.218	0.535	0.221	−0.447	−0.486	−0.423	−0.215	0.535	0.229

band. However, as noted above, the ALI was designed with a split band 4 and a new band 5′ in an attempt to improve on the ETM+ design. In Figs. 7(a) and 7(b) we illustrate the differences between the ALI and ETM+ bands in these 0.85 and 1.25 μm atmospheric windows, respectively. The light solid lines are the atmospheric transmission spectra in each window as calculated by 6S using our AERONET and TOMS measurements for the Rochester scene. In Fig. 7(a) the dashed line is the relative spectral response for the ETM+ band 4, which is clearly integrating over $\sim$10–35% water absorption between $\sim$0.81–0.84 μm. The dark solid lines show that the responses for the ALI bands 4 and 4′ were designed to avoid this absorption. In Fig. 7(b) the dark solid line shows the spectral bandpass for the new ALI band 5′, which has no counterpart in the ETM+.

We begin by examining the noise levels in each of the ETM+ and ALI bands. Since our goal is to understand the spectral information content when observing real surface targets, we will characterize the noise in the atmospherically corrected reflectance data as measured within a scene. This *in situ* noise assessment requires a suitably extended and uniform target, and is in contrast to pre-launch and on-orbit noise monitoring that measures the dark current for each detector when a shutter is blocking the instrument aperture.[7] Fortunately, the Rochester images contain a wide expanse of Lake Ontario extending to the Canadian shore that is suitable for a first-order noise assessment. However, we could not find an area in the lake that was featureless in each band across the entire 320 detectors of the ALI sensor chip assembly #4 used here, so we will quote reflectance noise levels to just a single significant digit or less. We find the ETM+ noise levels (1σ) in the reflectance images are approximately 0.002 for bands 2, 3, 4, and 7, but improve to roughly 0.001 in band 5 and are higher in band 1 at about 0.003. Similarly we assess the noise levels in ALI bands 1′ and 1 to be approximately 0.001, but improve to roughly

0.0005 in the rest of the bands. Thus we find that the ALI reflectance noise levels are approximately 2× to 4× lower than those in the ETM+ images. Further we note that the ALI noise levels should be considered upper limits because real features in the lake will raise the rms deviations from the mean reflectance values.

We now extract reflectance spectra from sample sites in both the Rochester and Howland scenes to quantitatively compare the multispectral bands of the ETM+ and ALI sensors. From the Rochester scene we extracted 4 pixels from a reasonably uniform grassy field, which we judged by eye to be common between the scenes, and in Fig. 8(a) we plot the mean reflectance spectra from each sensor. For Fig. 8(b) we similarly plot the average of $\sim$25 points from a nearby forest area, while in Fig. 8(c) we compare forest spectra extracted from 46 pixels in the Howland scene. We extracted multiple pixels in each case to average over differences in pixel alignment and to allow for differences in the MTF of each sensor. We find the overall agreement is very good for both the grass and forest regions. All bands except band 1 agree to within $\sim$5%, and the agreement in the SWIR (bands 5 and 7) is $\sim$2%. For the grass spectra the percent difference in band 1 is $\sim$6%, but this is only an absolute reflectance difference of $\sim$0.004, or roughly 1σ. This difference grows to $\sim$19% for the forest spectra in Rochester and $\sim$27% in Howland, but the absolute reflectance differences are just $\sim$0.004 and $\sim$0.007, respectively, so the much larger percentage differences are due to the very low reflectance in band 1 for forest regions. We find that the formal uncertainty in these reflectance spectra due to the 6S atmospheric correction process is at most $\sim$1.5%, as evaluated by the sensitivity study described in Section 2.3. The uncertainty is largest in the shortest wavelength bands, due to the larger path radiance, and decreases to less than 0.5% in bands 5 and 7. We note that the new ALI band 5′ provides additional sampling of the spectral shape for

Table 8 Principal components analysis of ETM+/ALI Bands 1, 2, 3, 4/4′, 5, and 7: loadings comparison for Howland, ME, scene.

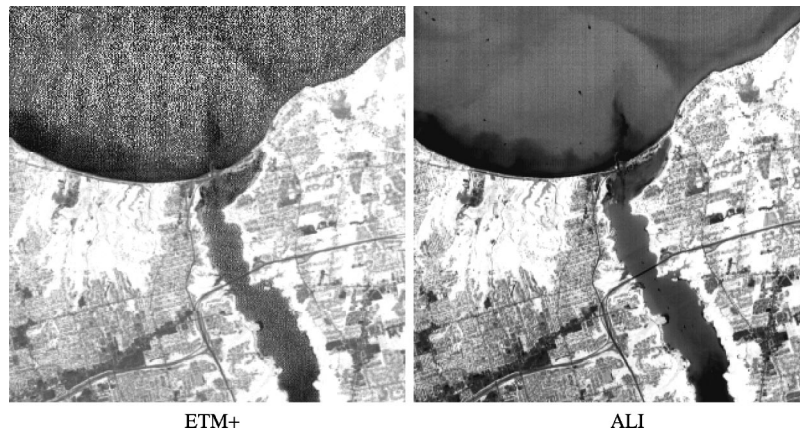| PCA Component	PCA Loadings for ETM+ Bands						PCA Loadings for ALI Bands					
	1	2	3	4	5	7	1	2	3	4′	5	7
1	0.025	0.076	0.058	0.864	0.454	0.192	0.021	0.071	0.048	0.883	0.425	0.179
2	−0.178	−0.209	−0.314	0.467	−0.585	−0.516	−0.189	−0.232	−0.341	−0.427	−0.579	−0.525
3	0.407	0.480	0.538	0.168	−0.528	0.088	0.417	0.483	0.522	0.175	−0.537	0.032

Fig. 9 Comparison of NDVI images: ETM+ (left) and ALI (right).

both the grass and forest regions. In particular, the ALI band 5′ measures near the peak of the grass reflectance spectrum, which is not sampled in the ETM+ data.

3.3 Information Content Comparisons

We are interested in comparing the spectral information content of the ETM+ and ALI data. We begin by considering information content in a generic sense by conducting a principal component analysis (PCA) of the ETM+ and ALI images. We compare the resulting orthogonal rotations in spectral space by examining both the eigenvalues and the eigenvectors (or component loadings). We then examine the information content for a specific application by comparing normalized difference vegetation index (NDVI) images derived from the ETM+ and ALI data.

We begin by performing PCA on the five bands that are most similar between the ETM+ and ALI, namely 1, 2, 3, 5, and 7. We initially exclude band 4 because of the different bandpasses [see Figure 7(a)]. In Tables 3 and 4 we show that the eigenvalues for the ALI and ETM+ are very similar in both the Rochester and Howland scenes. For both instruments we find that essentially all of the variation in both scenes can be captured with the first three principal components. Next we applied PCA to the six ETM+ bands and to ALI bands 1-3, 4′, 5, and 7. In Tables 5 and 6 we

again find that the variation explained by each component is very similar in each instrument for each scene. In Tables 7 and 8 we see that the close agreement between the two instruments extends to the eigenvectors (or loadings) themselves. These similarities in the PCA results indicate that for this landscape the ALI is able to reproduce the information content in the ETM+ images.

We further compare the information content of the two sensors by calculating the normalized difference vegetation index (NDVI) for the Rochester scene. The NDVI is a simple derived product often used to assess vegetation characteristics by calculating the normalized difference between the near infrared and red reflectance values. In Figs. 9 and 10 we show NDVI images and histograms calculated from the ETM+ data using bands 4 and 3, and from the ALI using the average of bands 4 and 4′ along with band 3. We see the two NDVI images are very similar over land, e.g., both histograms peak at an NDVI value of 0.88 due to vegetation. However, we see significant differences between the two sensors in water regions where the signal is very low. We clearly see black and white speckle in the ETM+ data for Lake Ontario, while the ALI is able to distinguish real details in the suspended sediments. The histogram for ETM+ shows this noise in the water as a tail in the distribution between -0.5 and 0.5, which corresponds to the ALI histogram counts between -0.2 and 0.3. We note that the peak in the ALI histogram at ~ 0.4 is real, since in Lake Ontario we find that the mean NIR reflectance is 0.0154 ± 0.001 (2σ) and the mean red reflectance is 0.0066 ± 0.001 (2σ), which give NDVI values of 0.4 ± 0.09. So, while the PCA shows the two sensors convey similar information, the NDVI images show the superior signal to noise of the ALI instrument because of its 12-bit quantization. Although we realize the NDVI is not typically used to analyze water targets, the ratio provides insight into the noise characteristics of the two sensors.
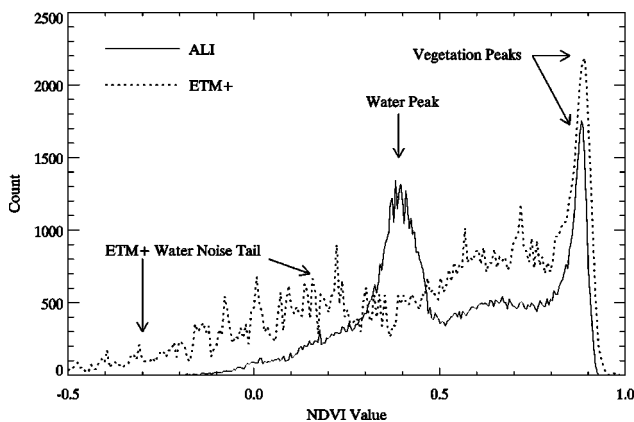
4 Conclusions

We have generated a set of atmospherically corrected, comparison images from the ETM+ sensor on Landsat-7 and the ALI instrument on EO-1 over tests sites in Rochester, New York, and Howland, Maine. We provided several il-

Fig. 10 Comparison of NDVI histograms.

lustrations of the relative consistencies and differences between the two space-borne sensors. We report 6S atmospheric correction coefficients for the ETM+ and ALI bands obtained from *in situ* Cimel sun photometers within the Aerosol Robotic Network. Reflectance spectra agree to within 6% in the visible/near infrared and to within 2% in the short-wave infrared (except for band 1 in dark forest targets). Uncertainties in atmospheric correction may account for at most 1.5% of these differences. Principal component analyses and comparison of NDVI histograms for each sensor indicate that the ALI is able to reproduce the information content in the ETM+ but with superior signal-to-noise performance with its increased 12-bit quantization.

Acknowledgments

References

1. S. G. Ungar, J. S. Pearlman, J. A. Mendenhall, and D. Reuter, "Overview of the Earth Observing One (EO-1) Mission," *IEEE Trans. Geosci. Remote Sens.* **41**, 1147–1159 (2003).
2. A. M. Mika, "Three decades of Landsat instruments," *Photogramm. Eng. Remote Sens.* **63**(7), 839–852 (1997).
3. B. L. Markham, J. L. Barker, J. A. Pedelty, I. Gorin, and E. Kaita, "Pre-launch performance of the Landsat-7 Enhanced Thematic Mapper Plus," *Proc. SPIE* **3439**, 40–48 (1998).
4. E. F. Vermote, D. Tanre, J. L. Deuze, M. Herman, and J.-J. Morcrette, "Second simulation of the satellite signal in the solar spectrum, 6S: An Overview," *IEEE Trans. Geosci. Remote Sens.* **35**, 675–686 (1997).
5. B. N. Holben, T. F. Eck, I. Slutsker, D. Tanre, J. P. Buis, A. Setzer, E. Vermote, J. A. Reagan, Y. J. Kaufman, T. Nakajima, F. Lavenu, I. Jankowiak, and A. Smirnov, "AERONET-a federated instrument network and data archive for aerosol characterization," *Remote Sens. Environ.* **66**, 1–16 (1998).
6. R. D. McPeters, P. K. Bhartia, A. J. Krueger, J. R. Herman, C. G. Wellemeyer, C. J. Seftor, G. Jaross, O. Torres, L. Moy, G. Labow, W. Byerly, S. L. Taylor, T. Swissler, R. P. Cebula, "Earth Probe Total Ozone Mapping Spectrometer (TOMS) Data Products User's Guide," NASA Technical Publication 1998-206895.
7. J. A. Pedelty, B. L. Markham, J. L. Barker, and J. C. Seiferth, "Pre-launch noise characterization of the Landsat-7 Enhanced Thematic Plus (ETM+)," *Proc. SPIE* **3750**, 376–387 (1999).

Jeffrey A. Pedelty received the BS degree in physics from the Iowa State University and the PhD degree in astrophysics from the University of Minnesota. He has worked on a variety of projects in his 15 years at NASA's Goddard Space Flight Center, including the COBE and Landsat-7 missions. His research interests include Earth remote sensing, radio astronomy, and computational science. Dr. Pedelty is a member of the SPIE, IEEE, and AAS.

Jeffrey T. Morisette received the BA in mathematics from Siena Heights College, the MS in applied statistics from Oakland University, and the PhD in forestry/remote sensing from North Carolina State University. His research interests include the application of multiresolution satellite imagery to ecological studies. He is chair of the Land Product Validation Subgroup of the Committeee on Earth Observing Satellite Working Group. Dr. Morisette is a member of the IEEE and AGU.

James A. Smith received the BS and MS degrees in mathematics and the PhD degree in physics from the University of Michigan and the MS degree in computer science from Johns Hopkins University. He is an editor of several SPIE conference proceedings on remote sensing, the editor of the SPIE Milestone volume on *Optical Remote Sensing: Theory and Measurement*, and a former editor of the *IEEE Transactions on Geoscience and Remote Sensing*. Dr. Smith is a senior fellow at NASA's Goddard Space Flight Center and a fellow of the SPIE, IEEE, and AAAS.